Available online at www.sciencedirect.com
ScienceDirect
Trans. Nonferrous Met. Soc. China 30(2020) 1031−1037
Transactions of Nonferrous Metals Society of China
www.tnmsc.cn

Effect of Eu^{3+}-doping on morphology and fluorescent properties of neodymium vanadate nanorod-arrays

Li TIAN[1,2,3,4], Shan-min CHEN[1,4], Qiang LIU[1,4], Jie-ling WU[1,4], Rui-ni ZHAO[3], Shan LI[1], Li-juan CHEN[1,4]

1. School of Materials Science and Engineering, Hunan University of Science and Technology, Xiangtan 411201, China;
2. Hunan Provincial Key Defense Laboratory of High Temperature Wear-resisting Materials and Preparation Technology, Xiangtan 411201, China;
3. Hunan Provincial Key Laboratory of Controllable Preparation and Functional Application of Fine Polymers, Xiangtan 411201, China;
4. Hunan Provincial Key Laboratory of Advanced Materials for New Energy Storage and Conversion, Xiangtan 411201, China

Received 24 May 2019; accepted 10 March 2020

Abstract: Tetragonal structural (t-$NdVO_4$) nanorod-arrays were fabricated by simple one-pot hydrothermal method. The phase, morphology and microstructure of $NdVO_4$ were characterized by X-ray diffractometer, scanning electron microscope (SEM), transmission electron microscope (TEM), dispersive X-ray spectrometer (EDS) and selected area electron diffraction (SAED) techniques. t-$NdVO_4$ nanorods are single-crystalline with a length of 100 nm and a diameter of 25 nm, which grow orientally along the direction of (112) crystalline plane and self-assemble to form nanorod-arrays. The results show that Eu^{3+}-doping interrupts the formation of $NdVO_4$ nanorod-arrays, and then leads to the red-shift of the strongest luminescence emission of Nd^{3+} transition from $^4D_{3/2}$ state to $^4I_{11/2}$ and decreases its intensity of the fluorescence emission at 400 nm sharply. The research results have some reference values to optimize the photoluminescence performance of rare earth vanadates.

Key words: Eu^{3+}-doping; morphology; fluorescent properties; neodymium vanadate; nanorod-arrays; hydrothermal method

1 Introduction

Rare earth vanadate nanomaterials possess the excellent physical and chemical properties owing to the unique 4f electronic structure. A variety of micro-topographies further expend their application range. At present, they have been extensively exploited in the fields of light, electricity, magnetism, catalysis, sensing and even infiltrated into other fields such as medical image science, biological probes and biological tags, showing broad application prospects in our daily lives [1,2]. The neodymium orthovanadate ($NdVO_4$) is an important member in rare earth vanadate functional materials, which has attracted a lot of attention from the international researchers recently because of its distinctive properties and potential application [3−6].

Having great novel photoelectric performances, $NdVO_4$ nanocrystals are suggested to use in the fields of imaging, biological labeling, detecting, and lasers [7−10]. It is well known that the fabrication methods of inorganic functional materials play an

Foundation item: Project (51202066) supported by the National Natural Science Foundation of China; Project (NCET-13-0784) supported by the Program for New Century Excellent Talents of the Education Ministry, China
Corresponding author: Li TIAN; Tel: +86-18627323439; E-mail: 1060072@hnust.edu.cn
DOI: 10.1016/S1003-6326(20)65274-8

important role in achieving the particular nanostuctures and novel morphology [11,12]. By far, there are different fabrication techniques to obtain $NdVO_4$ nanoparticles, for example, sonochemical operation, sol−gel preparation and microwave method [13−20]. YUVARAJ and KALAI [18] prepared $NdVO_4$ nanoparticles by sonochemical synthesis and studied the structural, magnetic and grain size dependent electrical properties. WU et al [19] obtained single-crystalline $NdVO_4$ nanorods by two-step stategy, and researched their emissions in the ultraviolet. FAN et al [20] synthesized the single-crystalline lanthanide orthovanadate nanorods by hydrothermal operation. However, the as-synthesized $NdVO_4$ nanorods are of different sizes and no $NdVO_4$ nanorod-arrays can be observed.

It is a challenge to obtain monodisperse $NdVO_4$ nanorods by simple preparation method. And $NdVO_4$ nanoarrays composed of monodisperse nanorods have not been reported so far. In this work, we prepared highly oriented t-$NdVO_4$ nanorod-arrays via a simple and controllable hydrothermal reaction process, particularly without hard or soft template. The synthesis method is reproducible. The crystalline phase, morphology and photoluminescence performance of the Eu^{3+}-doping $NdVO_4$ nanoarrays were studied. The effect of Eu^{3+}-doping on the crystalline phase and morphology of $NdVO_4$ nanoarrays was studied, showing that Eu^{3+}-doping interrupts the oriented-growth and self-assembly of $NdVO_4$ nanorods. And Eu^{3+}-doping leads to the red-shift of the strongest luminescence emission of Nd^{3+} transition from $^4D_{3/2}$ state to $^4I_{11/2}$ and decreases its intensity of the fluorescence emission at 400 nm sharply.

2 Experimental

2.1 Sample preparation

All chemicals including $Nd(NO_3)_3·6H_2O$, NH_4VO_3, NaOH and EDTA-2Na with analytic purity were not further purified before they were used. Typically, 0.428 g EDTA-2Na, 0.443 g $Nd(NO_3)_3·6H_2O$ and 5.0 mL distilled water were added into a beaker under vigorous stirring to form transparent solution. At the same time, 0.117 g NH_4VO_3 (1.0 mmol) was dissolved with 5.0 mL NaOH aqueous solution in another glass container. The resulting two kinds of solutions were poured into a Teflon-lined stainless steel autoclave of 20 mL capacity, and the pH value of the mixture was adjusted to 10 with NaOH aqueous solution. And then, the hydrothermal reaction temperature was kept constant at 180 °C for 24 h. The autoclave was cooled in air to room temperature after hydrothermal reaction. The precipitates were centrifuged, washed with deionized water and ethanol several times, and then dried in a vacuum oven. All Eu^{3+}-doping samples were prepared by the hydrothermal method under the same conditions. The Eu^{3+} contents were chosen to be 0, 1, 3, 5 and 7 wt.% in the NdVO4:Eu^{3+} samples, respectively.

2.2 Characterization

Powder X-ray diffractometer (XRD, Bucker D8 Advance) with Cu K_α radiation (λ=0.1541 nm) was used to characterize the phase of the products. The graphite monochromator was operated at 40 kV, 40 mA and a scanning speed of 10 (°)/min from 10 to 80 °C. The morphology and crystal structures of the $NdVO_4$ nanocrystals were characterized by scanning electron microscopy (SEM) images taken on a JEOL JSM−6330F field emission scanning electron microscope. The samples were gold-coated prior to the SEM analysis. The microstructure of $NdVO_4$ nanoarrays was further characterized by a JEM−2010HR transmission electron microscope (TEM). The accelerating operated voltage is 200 kV. The energy dispersive X-ray spectrum (EDS) was collected on an Oxford ISIS−300 energy dispersive X-ray spectrometer. Photoluminescence properties at room temperature were studied using PL spectrum with fluorescence spectrophotometer (F−4500). The products were excited by ultraviolet light obtained from xenon lamp with the excitation wavelength of 250 nm.

3 Results and discussion

3.1 Phase and crystal structures

The phase purity and crystal structures of the samples were characterized by powder X-ray diffractometry (XRD). Figure 1(a) shows the XRD pattern of as-prepared $NdVO_4$ nanorod-arrays. All the peaks can be well indexed to the tetragonal

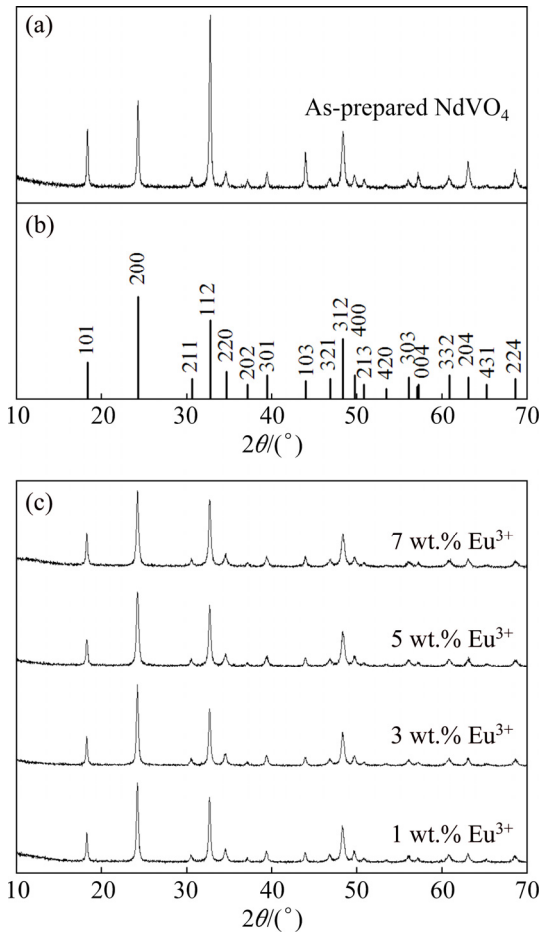

Fig. 1 XRD patterns of as-prepared $NdVO_4$ nanoparticles (a), standard sample of $NdVO_4$ (JCPDS No. 15−0769) (b) and as-prepared $NdVO_4$:Eu^{3+} with different contents of Eu^{3+} (c)

zircon-type structure of neodymium vanadium oxide ($NdVO_4$, JCPDS No. 15−0769) which has better photoluminescence performance than the samples with monazite-type structure [21], and the standard XRD pattern is shown in Fig. 1(b). As shown in Figs. 1(a) and (b), there are no other peaks found, indicating that highly-pure $NdVO_4$ can be achieved. Those sharp peaks in Fig. 1(a) indicate good crystallinity of the products. Compared with the standard card, the (200) and (112) diffraction peaks are observed to be different, revealing the orientation of crystal growth. In Fig. 1(a) the diffraction peak of (112) crystalline plane is higher and the diffraction peak of (200) crystalline plane is lower. Maybe it is related to the nanorod morphology and indicates the growth direction of (112) crystalline plane of $NdVO_4$ nanoarrays. The mean crystallite size of the as-synthesized of $NdVO_4$ nanoparticles is estimated by using the Scherrer equation to be 25 nm based on the FWHM (full-width at half maximum) of the (220) peak.

Ion-doping experiments were carried out to testify the effect of Eu^{3+}-doping on the crystalline phase, the morphology, the microstructure and the fluorescence of neodymium vanadate nanorod-arrays, keeping Eu^{3+} contents of $NdVO_4$:Eu^{3+} samples at 1, 3, 5 and 7 wt.%, respectively. The XRD patterns of the products are shown in Fig. 1(c). All the diffraction peaks shown in Fig. 1(c) are in agreement with the standard crystallographic data (JCPDS No. 15−0769) of tetragonal structural neodymium vanadium oxide ($NdVO_4$, space group $I41/amd$). That is to say, $NdVO_4$ can be gained and Eu^{3+}-doping has no distinct effect on the formation of tetragonal structural $NdVO_4$.

3.2 Morphology and microstructure

The morphology and microstructure of as-prepared $NdVO_4$ nanopaticles were examined by scanning electron microscopy. Figures 2(a−c) present the SEM images of as-obtained $NdVO_4$ nanorod-arrays with different magnifications. It is obvious that the $NdVO_4$ nanorods self-assemble to yield uniform nanoarrays. The higher magnification SEM images of neodymium vanadate nanoparticles shown in Figs. 2(b) and (c) indicate that $NdVO_4$ nanoarrays are composed of massive nanorods. The diameter of the nanorods is about 25 nm and the length is 100 nm or so. It is much smaller compared with the $NdVO_4$ nanorods synthesized by WU et al [19], which have rectangular cross-sections from about 30 nm × 30 nm to 100 nm × 200 nm and the length from 400 to 700 nm. This would be of great significance because of the possible novel properties induced by the reduced dimensionality and monodispersity.

Figure 2(d) gives the TEM image of $NdVO_4$ nanorod-arrays with ultrasonic treatment in need of TEM test, showing the self-assembly of $NdVO_4$ nanorods. It is clear that the nanorods still orient with a fine order. The SEAD pattern shown in Fig. 2(e) is obtained from the area circled in Fig. 2(d), indicating the growth direction of (112) crystalline plane and single-crystalline character of $NdVO_4$ nanorods.

Figure 3 displays the morphologies of the products prepared with different contents of Eu^{3+} being 1, 3, 5 and 7 wt.%, respectively. When

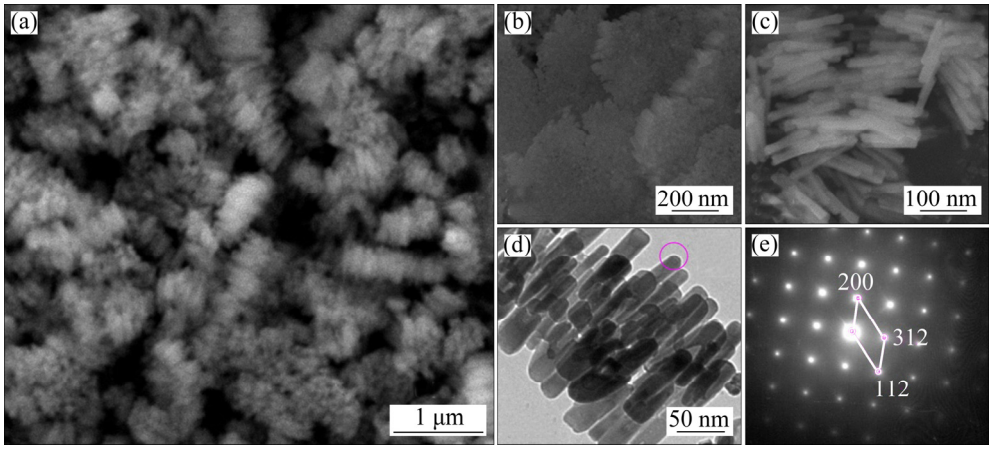

Fig. 2 SEM images with different magnifications (a, b, c) and TEM image (d) of as-prepared $NdVO_4$ nanorod-arrays, and SAED pattern of $NdVO_4$ nanorod (e) obtained from area circled in Fig. 2(d)

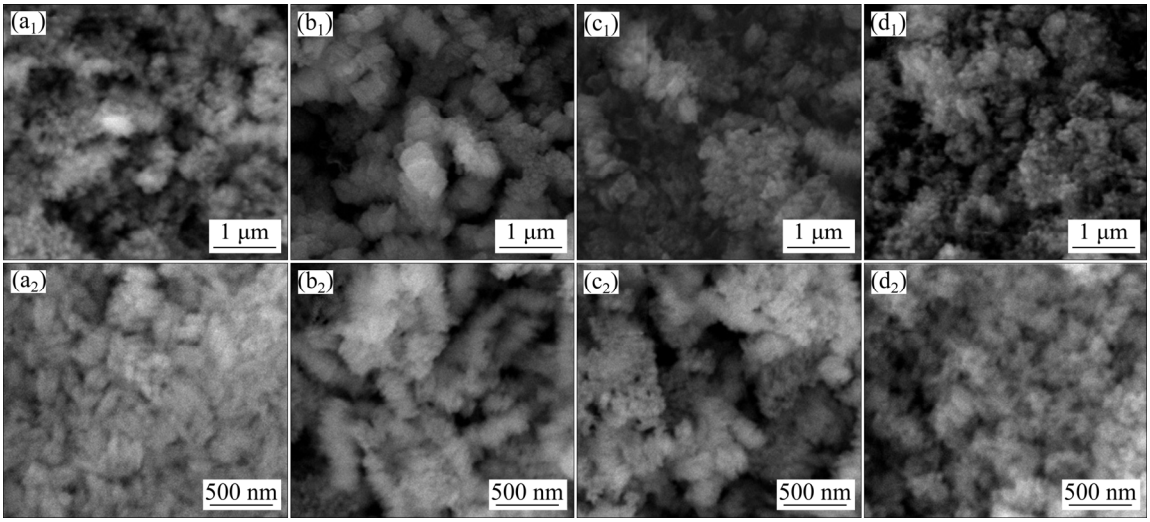

Fig. 3 SEM images of $NdVO_4$ nanoparticles prepared with different Eu^{3+}-doping contents at different magnifications: (a_1, a_2) 1 wt.%; (b_1, b_2) 3 wt.%; (c_1, c_2) 5 wt.%; (d_1, d_2) 7 wt.%

Eu^{3+} is doped into the reaction system, it is clear that no $NdVO_4$ nanorod-arrays are found. And the $NdVO_4$ nanoparticles in Fig. 3 are all in a mess and out of order. It is indicated that Eu^{3+}-doping interrupts the self-assembly of $NdVO_4$ nanorods and is unfavorable for the formation of $NdVO_4$ nanorod-arrays. The destructive behavior of Eu^{3+}-doping to the morphology of $NdVO_4$ nanorod-arrays maybe influence their photoluminescence (PL) performance.

Figure 4 shows the EDS spectra of $NdVO_4$ nanoparticles without Eu^{3+}-doping and with the Eu^{3+}-doping contents of 3 and 7 wt.%, respectively. Without Eu^{3+}-doping, the detected Nd/V/O mole ratio of $NdVO_4$ nanorod-arrays is about 1/1/4. When Eu^{3+} is doped into the reaction system, no oriented $NdVO_4$ nanorod-arrays are found as shown in Fig. 3, showing the effect of Eu^{3+}-doping on the formation and the morphology of $NdVO_4$ nanocrystals. In the EDS patterns of the samples synthesized with Eu^{3+}-doping, there is no obvious Eu signal detected. But from the EDS data, we find the Eu^{3+} mole fraction of 0.38% in the product prepared with Eu^{3+}-doping content of 7 wt.%. It is suggested that lower content of Eu^{3+} cannot be detected by EDS in this work.

3.3 Photoluminescence performance

The photoluminescence (PL) properties of $NdVO_4$ nanoparticles are recorded by fluorescence spectrometer at room temperature. Figure 5 shows the PL spectra of the samples without Eu^{3+}-doping

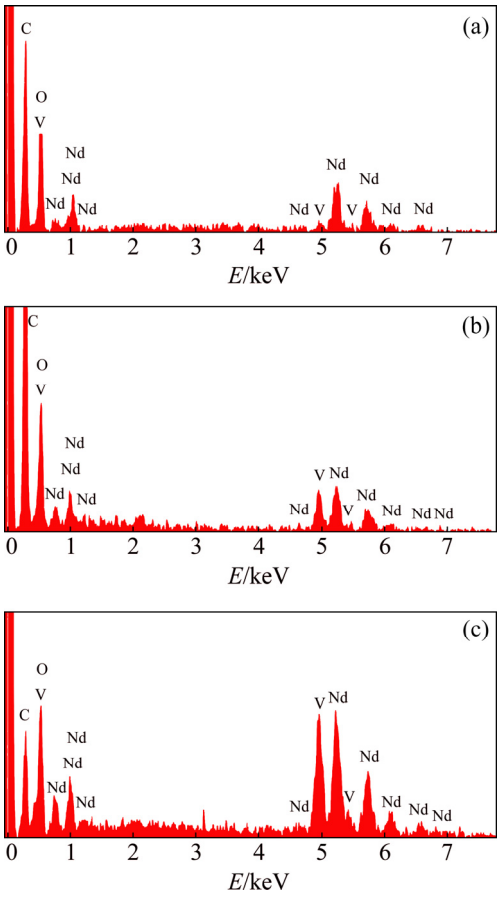

Fig. 4 EDS spectra of as-prepared $NdVO_4$ nanorod-arrays without Eu^{3+}-doping (a) and with Eu^{3+}-doping contents of 3 wt.% (b) and 7 wt.% (c)

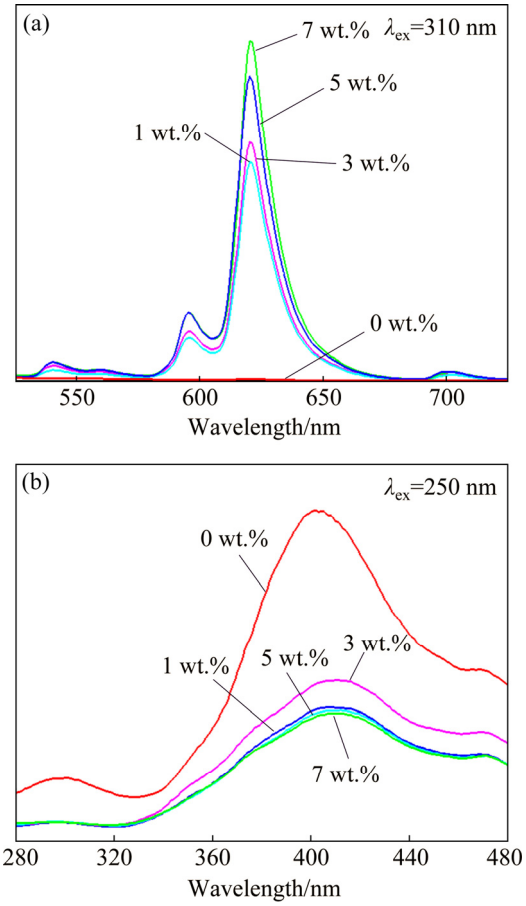

Fig. 5 Photoluminescence spectra of as-prepared $NdVO_4$:Eu^{3+} without Eu^{3+}-doping and with different Eu^{3+}-doping contents: (a) Emission spectra between 525 and 725 nm with excitation wavelength of 310 nm; (b) Emission spectra between 280 and 480 nm with excitation wavelength of 250 nm

and with different Eu^{3+}-doping amounts of 1, 3, 5 and 7 wt.%. As shown in Fig. 5(a), a number of sharp emission peaks occur in the wavelength region from 525 to 725 nm, with the excitation wavelength of 310 nm. The emssion bands of $NdVO_4$:Eu^{3+} are associated with the f−f transitions (around 540 and 559 nm) and $^5D_0$–$^7F_1$ (around 595 nm), $^5D_0$–$^7F_2$ (around 620 nm), $^5D_0$–$^7F_3$ (around 702 nm) transitions of Eu^{3+} [22]. From the results, the variation trend of the samples with different Eu^{3+}-doping amounts is the same. The integrated intensity increases gradually with the Eu^{3+}-doping content increasing to 7 wt.%. This indicates that more Eu^{3+} ions are incorporated into the host lattice at a higher Eu^{3+}-doping content (7 wt.%) and prominent energy migration between the Eu^{3+} ions takes place. The mission intensity of $^5D_0 \rightarrow {}^7F_j$ depends on the amount of Eu^{3+} [23].

To identify the effect of Eu^{3+}-doping on the photoluminescence performance of $NdVO_4$, Fig. 5(b) shows the emission spectra of the samples in the wavelength region from 280 to 480 nm excited by 250 nm. There are two distinct luminescence emission peaks observed, one weak peak at 300 nm and the other strong peak at 400 nm, if no Eu^{3+} ions are doped in the reaction system. Because $NdVO_4$ nanocrystals are composed of Nd^{3+} and VO_4^{3-}, the weak peak at 300 nm (4.2 eV) is most likely a result of the electron transition in VO_4^{3-}, which corresponds to electron transition from O 2p nonbonding state to V 3d and O 2p antibonding states. The strong emission peak at 400 nm can be attributed to Nd^{3+} transition from the $^4D_{3/2}$ state to $^4I_{11/2}$.

At the same time, two extraordinary weak luminescence emission peaks can been detected at 352 and 467 nm which are assigned to Nd^{3+} transitions from the $^4D_{3/2}$ and $^4G_{11/2}$ states to $^4I_{9/2}$, respectively. When Eu^{3+} ions are doped in the

reaction system and interrupt the formation of $NdVO_4$ nanorods, the intensity of the strongest emission peak decreases sharply, indicating the quench effect of Eu^{3+} on the fluorescence properties of $NdVO_4$ nanocrystals. In addition, it can be found that the strongest emission peak of 400 nm has some red-shift to 412 nm, showing the change of Nd^{3+} transition from the $^4D_{3/2}$ state to $^4I_{11/2}$, owing to the doping of Eu^{3+}. As we all know, the size of Eu^{3+} is smaller than that of Nd^{3+}. When $NdVO_4$ nanocrystals are doped by Eu^{3+} with smaller size, the lattice constant decreases and the intensity of crystal field increases. Generally, the photo-luminescence emission peak of rare earth vanadates has some red-shift due to the increasing intensity of crystal field [24]. The study on the detailed relation between crystal structure and photoluminescence performance is under way.

4 Conclusions

(1) Tetragonal structural $NdVO_4$ nanoarrays composed of monodisperse nanorods were prepared by simple and reproducible hydrothermal methods.

(2) $NdVO_4$ nanoparticles are testified to grow orientally along the direction of (112) crystalline plane to form tetragonal structural $NdVO_4$ nanorods with the mean length of 100 nm and the diameter of 25 nm. Tetragonal structural $NdVO_4$ nanorods show single-crystalline character and self-assemble into $NdVO_4$ nanoarrays.

(3) Eu^{3+}-doping has no effect on the crystalline phase of $NdVO_4$ nanoarrays, but interrupts the oriented-growth and self-assembly of $NdVO_4$ nanorods. $NdVO_4$ nanorod arrays prepared exhibit strong luminescence emission at 400 nm attributed to Nd^{3+} transition from the $^4D_{3/2}$ state to $^4I_{11/2}$. The strongest luminescence emission at 400 nm has red-shift to 412 nm with sharp decrease of the fluorescence emission intensity due to the Eu^{3+}-doping. It is indicated an interruption of Eu^{3+}-doping to the morphology of $NdVO_4$ nanoarrays and a quench effect of Eu^{3+} on the fluorescence property of $NdVO_4$ nanoarrays, which is of a certain significance to optimize the photo-luminescence performance of rare earth vanadates.

References

[1] PETROV D. Lattice enthalpies of lanthanide orthovanadates $LnVO_4$ [J]. Croatica Chemica Acta, 2013, 1: 85−87.

[2] TIAN Li, ZHAO Rui-ni, WANG Jing-jing, CHEN Lin, XUE Jian-rong, XIAO Qiu-guo. Formation mechanism and luminescence properties of nanostructured sodium yttrium fluoride corn sticks synthesized by precipitation transformation method [J]. Journal of Rare Earths, 2015, 33: 1246−1250.

[3] MIRELA D, MATJAZ V. Room-temperature synthesis and optical properties of $NdVO_4$ nanoneedles [J]. Acta Chimica Slovenica, 2018, 65: 679−673.

[4] PANCHAL V, ERRANDONE D, MANJON F J, MUNOZ A, RODRIGUEZ H P, ACHARY S N, TYAGI A K. High-pressure lattice-dynamics of $NdVO_4$ [J]. Journal of Physics and Chemistry of Solids, 2017, 100: 126−130.

[5] ROZITA M, MARYAM G, MASOUD S N. Utilizing of neodymium vanadate nanoparticles as an efficient catalyst to boost the photocatalytic water purification [J]. Journal of Environmental Management, 2019, 230: 266−269.

[6] LI Wei, FANG Liang, SUN Yi-hu, TANG Ying, CHEN Jin-wu, LI Chun-chun. Preparation, crystal structure and microwave dielectric properties of rare-earth vanadates: $ReVO_4$ (Re=Nd, Sm) [J]. Journal of Electronic Materials, 2017, 4: 46−49.

[7] KACZMAREK S M, BERKOWSKI M, LENIEC G, GLOWACKI M M, SKIBINSKI T. EPR properties of concentrated $NdVO_4$ single crystal system [J]. Applied Magnetic Resonance, 2015, 46: 1023−1027.

[8] TIAN Li, LI Yan, WANG Hui-fang, CHEN Shan-min, WANG Jin-jing, GUO Zhen, LIU Qiang, LUO Qi, LI Ying-jie, WU Fa-fa. Controlled preparation and self-assembly of $NdVO_4$ nanocrystals [J]. Journal of Rare Earths, 2018, 36: 179−181.

[9] CHIANG T, CHEN T. Photocatalytic water splitting for O_2 production under visible light irradiation using $NdVO_4$−V_2O_5 hybrid powders [J]. Materials, 2017, 10: 331−336.

[10] ROSAL B, PEREZ D A, CARRASCO E, JOVANOVIC D J. DRAMICANIN M D, GORAN D, SANZ R F, JAQUE D. Neodymium-based stoichiometric ultrasmall nanoparticles for multifunctional deep-tissue photothermal therapy [J]. Advanced Optical Materials, 2016, 4: 782−786.

[11] CHEN Li-juan, FENG Tao, WANG Peng-fei, CHEN Zi-wen, YAN Ri-qing, LIAO Bo, XIANG Yu-jun. A recorverable sandwich phosphorotungstate stabilized palladium(0) catalyst for aerobic oxidation of alcohols in water [J]. Applied Catalysis A: General, 2016, 523: 304−311.

[12] XU Jun-na, CHEN Xiao-qing, GAO Xiong, ZHOU you-yuan, XIAO Ke-song, HUANG Chen-huan, XI Xiao-ming. Structure and electrochemical performance of yttrium oxide coated $LiNi_{0.5}Co_{0.2}Mn_{0.3}O_2$ [J]. Electrochimica Acta, 2018, 228(3): 528−532.

[13] SELVAN R K, GEDANKEN A, ANILKUMAR P, MANIKANDAN G, KARUNAKARAN C. Synthesis and characterization of rare earth orthovanadate (RVO_4; R=La, Ce, Nd, Sm, Eu, Gd) nanorods/nanocrystals/nanospindles by a facile sonochemical method and their catalytic properties [J]. Journal of Cluster Science, 2014, 2: 291−305.

[14] ROZITA M, MARYAM G, MASOUD S. Application of ultrasound-aided method for the synthesis of $NdVO_4$ nano-photocatalyst and investigation of eliminate dye in

contaminant water [J]. Ultrasonics Sonochemistry, 2018, 42: 201−207.

[15] CHEN Peng-fei, WU Qiang, ZHANG Li, YAO Wei-feng. Facile immobilization of $LnVO_4$ (Ln = Ce, Nd, Gd) on silica fiber via a combined alcohol-thermal and carbon nanofibers template route [J]. Catalysis Communications, 2015, 66: 6−12.

[16] VOSOUGHIFAR M. Synthesis, characterization and investigation on magnetic and photocatalytic property of neodymium vanadate nanoparticles [J]. Journal of Materials Science: Materials in Electronics, 2016, 27: 7384−7389.

[17] KHADEMOLHOSEINI S, GOUDARZI M. New approach to synthesize nanocrystalline $NdVO_4$ in the presence of carbohydrates as capping agent [J]. Journal of Materials Science: Materials in Electronics, 2017, 28: 1449−1456.

[18] YUVARAJ S, KALAI S R. Sonochemical synthesis, structural, magnetic and grain size dependent electrical properties of $NdVO_4$ nanoparticles [J]. Ultrasonics Sonochemistry, 2014, 21: 599−604.

[19] WU Xing-cai, TAO You-yong, DONG Lin, ZHU Jun-jie, HU Zheng. Preparation of single-crystalline $NdVO_4$ nanorods, and their emissions in the ultraviolet and blue under ultraviolet excitation [J]. The Journal of Physical Chemistry B, 2005, 109: 11544−11548.

[20] FAN Wei-liu, ZHAO Wei, YOU Li-ping, SONG Xin-yu, ZHANG Wei-ming, YU Hai-yun, SUN Si-xiu. A simple method to synthesize single-crystalline lanthanide orthovanadate nanorods [J]. Journal of Solid State Chemistry, 2004, 177: 4399−4406.

[21] FAN Wei-liu, SONG Xin-yu, YU,Xiang, SUN Si-xiu, ZHAO Xian. Selected-control hydrothermal synthesis and formation mechanism of monazite and zircon-type $LaVO_4$ nanocrystals [J]. The Journal of Physical Chemistry B, 2006, 110: 23247−23252.

[22] WEI Zheng-gui, SUN Ling-dong, LIAO Chun-sheng, YAN Chun-hua, HUANG Shi-hua. Fluorescence intensity and color purity improvement in nanosized YBO_3:Eu [J]. Applied Physics Letters, 2002, 80: 1447−1449.

[23] QUAN Yu, LIU Su-qin, HUANG Ke-long, FANG Dong, ZHANG Xue-ying, HOU Hua-wei. Hydrothermal synthesis and characterization of Eu-doped GaOOH/α-Ga_2O_3/β-Ga_2O_3 nanoparticles [J]. Transactions of Nonferrous Metals Society of China, 2010, 20: 1458−1462.

[24] LIU Guo-cong, DUAN Xue-chen, LI Hai-bin, DONG Hui. Hydrothermal synthesis, characterization and optical properties of novel fishbone-like $LaVO_4$:Eu^{3+} nanocrystals [J]. Materials Chemistry and Physics, 2009, 115: 165−172.

Eu^{3+}掺杂对钒酸钕纳米棒阵列形貌和荧光性能的影响

田 俐[1,2,3,4]，陈善民[1,4]，刘 强[1,4]，吴杰灵[1,4]，赵瑞妮[3]，黎 珊[1]，陈丽娟[1,4]

1. 湖南科技大学 材料科学与工程学院，湘潭 411201；
2. 湖南省高温耐磨材料与制备技术重点防御实验室，湘潭 411201；
3. 湖南省精细聚合物可控制备与功能应用重点实验室，湘潭 411201；
4. 新能源储存与转换先进材料湖南省重点实验室，湘潭 411201

摘 要：采用简单一锅水热法制备具有四方晶相的 $NdVO_4$(t-$NdVO_4$)纳米棒阵列。通过 X 射线粉末衍射仪(XRD)、扫描电子显微镜(SEM)、透射电子显微镜(TEM)、X 射线能谱仪(EDS)和选区电子衍射(SAED)技术对 t-$NdVO_4$ 纳米棒阵列的物相、形貌和显微组织进行表征。所制备的 t-$NdVO_4$ 纳米棒为单晶，长度约为 100 nm，直径为 25 nm，并且沿(112)晶面方向定向生长、自组装而成纳米棒阵列。研究表明，Eu^{3+}掺杂会影响 $NdVO_4$ 纳米棒阵列的形成，并导致 Nd^{3+}从 $^4D_{3/2}$ 状态到 $^4I_{11/2}$ 的最强光发射红移，并且在 400 nm 处急剧降低其荧光发射强度。研究结果对优化稀土钒酸盐的光致发光性能具有一定的参考价值。

关键词：Eu^{3+}掺杂；形貌；荧光性能；钒酸铵；纳米棒阵列；水热合成

(Edited by Wei-ping CHEN)